FINAL REVISION: 4/8/02

Static Microfield Printing at the Advanced Light Source with the ETS Set-2 Optic

Patrick P. Naulleau[1], Kenneth A. Goldberg[1], Erik H. Anderson[1], David Attwood[2], Phillip Batson[1], Jeffrey Bokor[1,2], Paul Denham[1], Eric Gullikson[1], Bruce Harteneck[1], Brian Hoef[1], Keith Jackson[1], Deirdre Olynick[1], Seno Rekawa[1], Farhad Salmassi[1], Ken Blaedel[3], Henry Chapman[3], Layton Hale[3], Regina Soufli[3], Eberhard Spiller[3], Don Sweeney[3], John Taylor[3], Chris Walton[3], Avijit Ray-Chaudhuri[4], Donna O'Connell[4], Richard Stulen[4], Daniel Tichenor[4], Charles W. Gwyn[5], Pei-Yang Yan[5], and Guojing Zhang[5]

[1]Center for X-Ray Optics, Lawrence Berkeley National Laboratory, Berkeley, CA 94720
[2]EECS Department, University of California, Berkeley, CA 94720
[3]Lawrence Livermore National Laboratory, PO Box 808, Livermore, CA 94550
[4]Sandia National Laboratories, PO Box 969, Livermore CA 94551
[5]Intel Corporation, 2200 Mission College Boulevard, Santa Clara CA 95052

ABSTRACT

While interferometry is routinely used for the characterization and alignment of lithographic optics, the ultimate performance metric for these optics is printing in photoresist. The comparison of lithographic imaging with that predicted from wavefront performance is also useful for verifying and improving the predictive power of wavefront metrology. To address these issues, static, small-field printing capabilities have been added to the EUV phase-shifting point diffraction interferometer (PS/PDI) implemented at the Advanced Light Source at Lawrence Berkeley National Laboratory. The combined system remains extremely flexible in that switching between interferometry and imaging modes can be accomplished in approximately two weeks.

Relevant printing studies with the ETS projection optics require illumination partial coherence with σ of approximately 0.7. However, this σ value is very different from the coherent illumination naturally provided by synchrotron undulator beamline and required by the high accuracy EUV PS/PDI. Adding printing capabilities to the PS/PDI experimental system has thus necessitated the development of an alternative illumination system capable of quantitatively reducing the inherent coherence of the beamline. The implemented illuminator is an angular scanning system capable of *in situ* coherence control. Moreover, this illuminator design readily enables the implementation of conventional resolution-enhancing pupil fills and modeling of the unique Engineering Test Stand (ETS) pupil fill.

This new static microfield exposure tool has been used to lithographically characterize the static imaging performance of the ETS Set-2 projection optics. Excellent performance has been demonstrated down to the 70-nm 1:1 line/space level with a focus latitude exceeding 1 μm and a dose latitude of approximately 8%. Moreover, dense-line printing down to a resolution of 50 nm has been demonstrated.

Keywords: extreme ultraviolet lithography, synchrotron radiation, microfield printing, decoherentizing illuminator

Contact: P. Naulleau; Email: Pnaulleau@lbl.gov; Tel: 510-486-4529; Fax: 510-486-4550

1. INTRODUCTION

Extreme ultraviolet (EUV) projection lithography is now the leading contender for *next-generation lithography* beyond the limits imposed by currently used refractive optical systems. Because EUV systems utilize resonant reflective coatings,[1] at-wavelength characterization,[2] including system wavefront metrology, has played an essential role in the development of EUV lithographic optics.

To meet the at-wavelength wavefront metrology challenge, an EUV-compatible diffraction-class interferometer, the phase-shifting point diffraction interferometer (PS/PDI), has been developed and implemented at Lawrence Berkeley National Laboratory.[3] The PS/PDI has been demonstrated to have a wavefront measurement accuracy of better than $\lambda_{EUV}/200$ (0.67 Å) within a numerical aperture (NA) of 0.1.[4]

While PS/PDI wavefront interferometry[5-7] is now routinely used for the characterization and alignment of EUV lithographic optics,[8,9] the ultimate performance metric for lithographic systems is printing in photoresist. Direct comparison of imaging and wavefront performance is also useful for verifying and improving the predictive power of wavefront metrology under actual printing conditions. To address these issues in the most flexible and time-efficient manner, static, microfield printing capabilities have been added to the EUV PS/PDI. In printing configuration, the test station is referred to as the Static Exposure Station (SES). This at-wavelength test station has been designed to test the 4×-reduction projection optics boxes[9] developed for implementation in the EUV Engineering Test Stand (ETS)[10] now operational at the Virtual National Laboratory (the VNL is a partnership between Lawrence Berkeley, Lawrence Livermore, and Sandia National Laboratories).

Two EUV 4×-reduction optical systems have been developed as part of the EUV LLC's EUV lithography program with the first developmental set of optics (the Set-1 optic) currently operating in the ETS.[11] As described in this manuscript, the second much higher quality optic[4,12] (the Set-2 optic) is currently undergoing microfield static printing characterization in the SES. Although this optic is destined for integration into the ETS for full-field scanned imaging, valuable early learning has been obtained by the new microfield static printing capabilities of the SES.

A static imaging system, the SES has a microfield size of approximately 100 μm at the wafer. However, the full 1-inch arc field can be covered one microfield at a time by moving the entire system relative to the stationary illumination beam. The SES works with the same reflection masks used in the ETS. In addition, the SES supports variable partial coherence (σ) ranging from approximately 0 to 1 as well as enabling a lossless programmable pupil fill.

The biggest challenge for the implementation of printing capabilities at the EUV interferometry beamline was modifying the illumination coherence. Relevant printing studies with lithographic optics require illumination partial coherence (σ) of approximately 0.7. This σ value is very different from the coherent illumination requirements of the EUV PS/PDI and the coherence properties naturally provided by synchrotron undulator beamline illumination (<0.05).[13,14] Adding printing capabilities to the PS/PDI experimental system has thus necessitated the development of a novel illumination system capable of quantitatively reducing the inherent coherence of the beamline.

2. ADDING PRINTING CAPABILITIES TO THE PS/PDI

Although the illumination issue is the most fundamental of the changes required to implement printing in the EUV interferometry tool, several other modifications were necessary to enable printing in a system originally designed for interferometry. These modifcations have been previously described in detail[15] and are briefly summarized here.

In contrast to the transmission configuration of the PS/PDI,[3] relevant printing studies require a reflection mask (reticle) to be used and, therefore, the illumination must come from below the object plane. This is achieved by providing clearance for the beam to pass downward through the object plane before it is redirected upward to illuminate the reflection reticle (Fig. 1). The final illuminator optic used to redirect the beam upward is positioned at the location normally occupied by the PS/PDI grating.

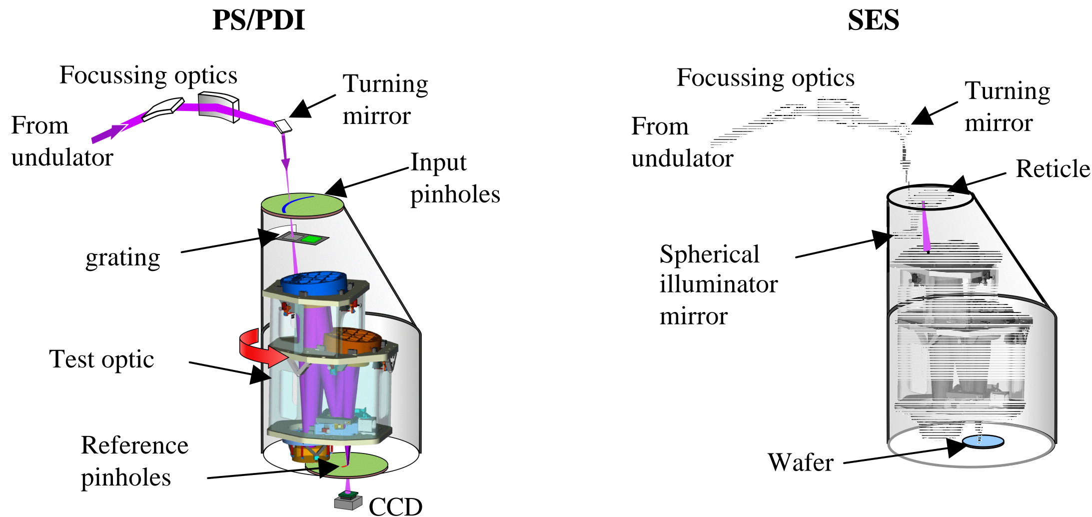

Fig. 1. Schematic of at-wavelength system characterization test stand in both PS/PDI and SES modes. PS/PDI endstation in interferometry mode. In SES mode, the beamline illumination passes through the object plane and is redirected upward using a spherical mirror that replaces grating used in interferometry mode.

Another important issue for the SES was image-plane-stage speed. The original flexural, picomotor-driven stage design was optimized for extremely high resolution (better than 10 nm) at the expense of speed (the original stage speed was approximately 1 μm/s). In imaging mode with no overlay capabilities, however, stage resolution is not important, although stage speed is in order to enable the acquisition of focus-exposure matrices (FEM) in a reasonable amount of time. To address the lateral-scanning speed issue a nested-stage solution has been implemented providing a 20× increase in stage speed while maintaining accuracy when required. This new stage design enables the acquisition of large FEMs (13×13) in approximately 1 hour.

Also newly implemented for printing operation were an electrostatic chuck for the wafer and a vacuum load-lock wafer-transfer system.

3. ILLUMINATOR

As stated above, illumination was the most fundamental concern for implementing lithographic printing capabilities on a beamline optimized for the high spatial coherence demanded by high-accuracy wavefront metrology. This issue has been addressed by implementing an active illumination system as shown in Fig. 2. In this system, the final illuminator mirror (as shown in Figs. 1 and 2) is a spherical mirror designed to re-image the beamline turning mirror to the reticle. The turning mirror is an active component that can be scanned in angle in two dimensions.

In this illuminator the angular scanning mirror serves as the effective source that is re-imaged to the reticle by way of the spherical mirror; thus it is a *critical* illumination system. By scanning the mirror comprising the effective source in angle, the source spatial-frequency content can be arbitrarily defined. Noting that the spatial coherence properties of a source are simply related to the Fourier transform of the source spatial spectrum (Van Cittert-Zernike Theorem),[16] it

is evident that the illumination coherence properties can be controlled through the definition of the source scanning.

Alternatively this illuminator can be described from the pupil-fill perspective. Because this is a *critical* illumination system, the lithographic optic pupil can be viewed as a Fourier-transform plane of the source, thus the pupil image is simply an image of the source spatial-spectral content. Scanning the source serves to “paint out” the pupil fill with a small dot representing the intrinsic coherence (or pupil fill) produced by the beamline. Again, it is evident that the illumination coherence properties (or pupil fill) can be synthesized through a source scanning pattern.

It is important to note that the coherence control described above assumes the observation time to be long relative to the scan rate. In practice this means that the lithographic exposure time should be at least as long as it takes to fully scan the desired pupil fill once. Additionally, the exposure time should be an integer multiple of the full pupil fill scan time. If this condition is not satisfied some portions of the pupil fill would receive higher weighting than others, thereby changing the coherence properties relative to the desired pupil fill.

In the case of a typical $\sigma = 0.7$ pupil fill in the SES, the full pupil scan time is approximately 1 second set by the mechanical resonance of the 2-D scanner. In practice we cycle through the pupil fill at least four times for improved uniformity; thus, a typical SES exposure is four seconds long. We note that were the scan time not a limiting factor, the undulator beamline would have enough power to support millisecond exposures in the 100-µm SES microfield. In the present condition, the beamline power is intentionally restricted.

Figure 3 shows a series of EUV pupil fills generated by the scanning system described above and recorded through the ETS Set-2 optic. A back-thinned back-illuminated EUV CCD camera is used to capture the pupil-fill images. The dashed lines represent the full 0.1 numerical aperture ETS optic pupil. These images demonstrate the wide variety of pupil fills (coherence functions) that can be generated, including resolution enhancing pupil fills. Another very important benefit of this

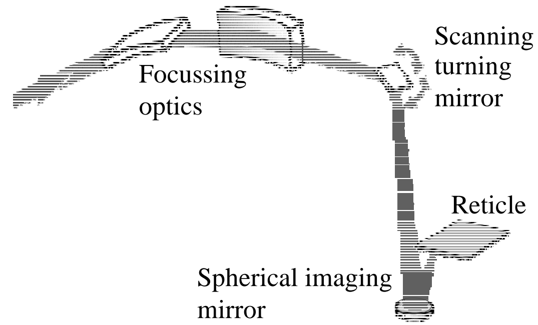

Fig. 2. Schematic of scanning-mirror SES illuminator. A spherical mirror re-images a 2-D angle scanning turning mirror, which serves as the effective source, to the reticle. The spatial bandwidth (coherence) of the effective source is synthesized through the scanning process.

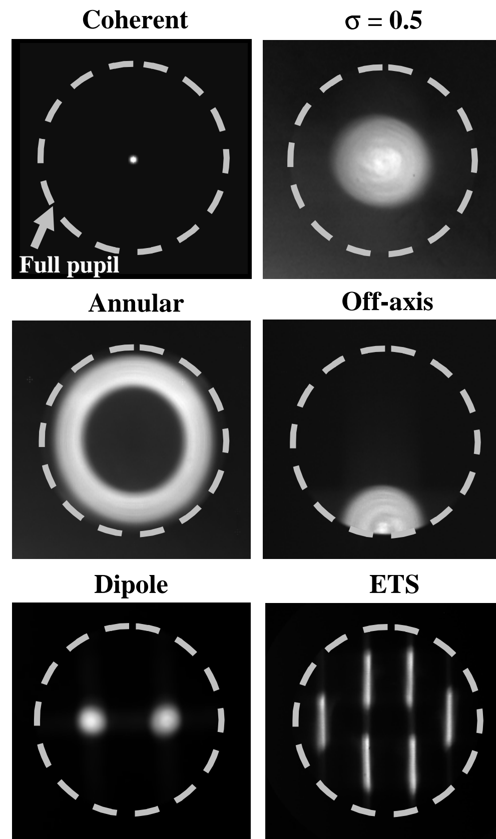

Fig. 3. Series of EUV pupil fills generated by the scanning system described above and recorded through the lithographic ETS Set-2 optic. A back-thinned back-illuminated EUV CCD camera is used to capture the pupil-fill images.

capability is the ability to model pupil fills used in other systems. For example, the final pupil fill image in Fig. 3 shows the ETS 6-Channel pupil fill. This level of control allows the SES to not only characterize the imaging performance of the Set-2 optic but it also enables the SES to investigate pupil-fill specific effects of the ETS or any other system-specific pupil fill.

4. PRINTING CHARACTERIZATION

The ETS Set-2 optic[9] is a 0.1 numerical aperture (NA) optic designed for 100-nm critical dimensions (CD). At the central field point, where all subsequent printing results are presented, the Set-2 optic has a wavefront quality of 0.69 nm or 52 mwaves. A detailed description of the interferometric characterization of the Set-2 optic can be found in Refs. 4 and 12. Figure 4 (lower line) shows the calculated binary-dense-line modulation transfer function (MTF) for the Set-2 optic assuming the measured central-field point wavefront and a partial coherence of 0.7. Other than a global reduction in contrast due to flare, comparison with an ideal 0.1-NA optic MTF (upper line in Fig. 4) shows the Set-2 optic to perform like a diffraction limited optic (at least in terms of the MTF). An initial roll-off is evident shortly after 100-nm CD with a much sharper roll-off starting around 70-nm CD.

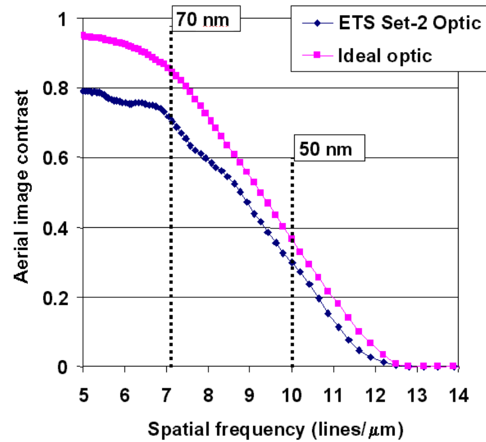

Fig. 4. Calculated binary-dense-line modulation transfer function (MTF) at the central field point assuming a partial coherence of 0.7.

Figure 5 shows a series of 100-nm CD images demonstrating the excellent printing performance of the Set-2 optic at its designed CD. With a NA of 0.1, 100-nm CD represents a k_1 factor of 0.75, where k_1 is defined as (CD)(NA)/λ. All images were recorded with conventional disk illumination and a partial coherence of 0.8. We note that with an NA of 0.25 (the expected NA of the first EUV Beta tools), an equivalent k_1 factor would yield a CD of 40 nm.

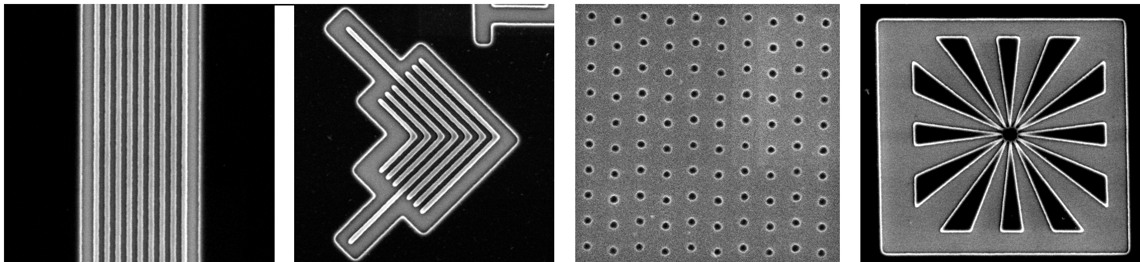

Fig. 5. Series of printed images at the Set-2 optic design CD of 100 nm. With a NA of 0.1, 100-nm CD represents a k_1 factor of 0.75. All images recorded with conventional disk illumination and a partial coherence of 0.8.

Although designed for 100-nm CD, as suggested by the MTF in Fig. 4, the Set-2 optic is capable of higher-resolution performance. Figure 6 shows a series of equal line-space images ranging from 90-nm CD down to 60-nm CD. All images were recorded with conventional disk illumination and a partial coherence of 0.8. Under conventional illumination, the Set-2 optic is seen to perform down to a k_1 factor of 0.45 on dense-line features. Process latitude studies at 70-nm dense-lines CDs has demonstrated a depth of focus of 1.2 μm and a dose latitude of 8%, where both values are based on a total 10% range about the nominal CD.

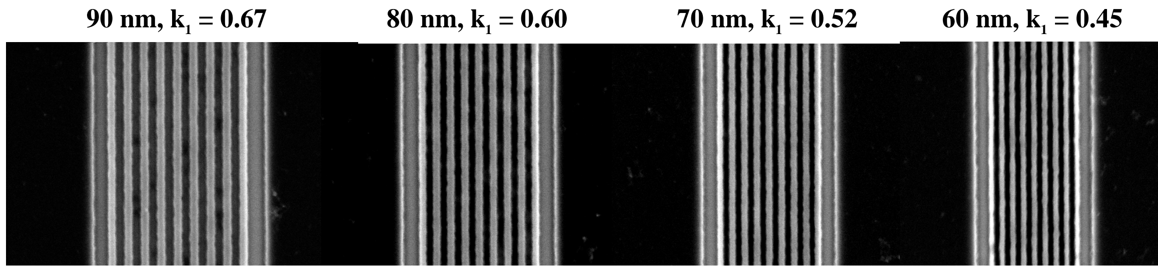

Fig. 6. Series of dense-line images ranging from 90-nm CD down to 60-nm CD. All images were recorded with conventional disk illumination and a partial coherence of 0.8.

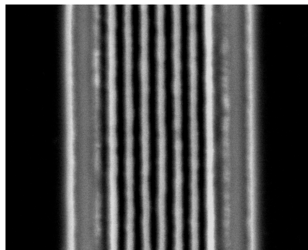

Fig. 7. 50-nm dense line printing (k_1 = 0.37) achieved with dipole illumination.

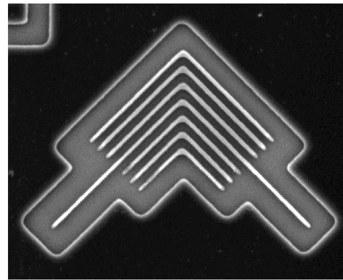

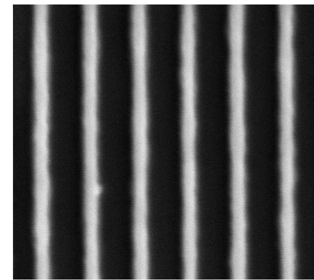

Fig. 8. 39-nm 3:1 pitch elbows and lines printed by overdosing features coded as 80-nm 1:1 on the reticle. Conventional disk illumination with a σ of 0.7 was used.

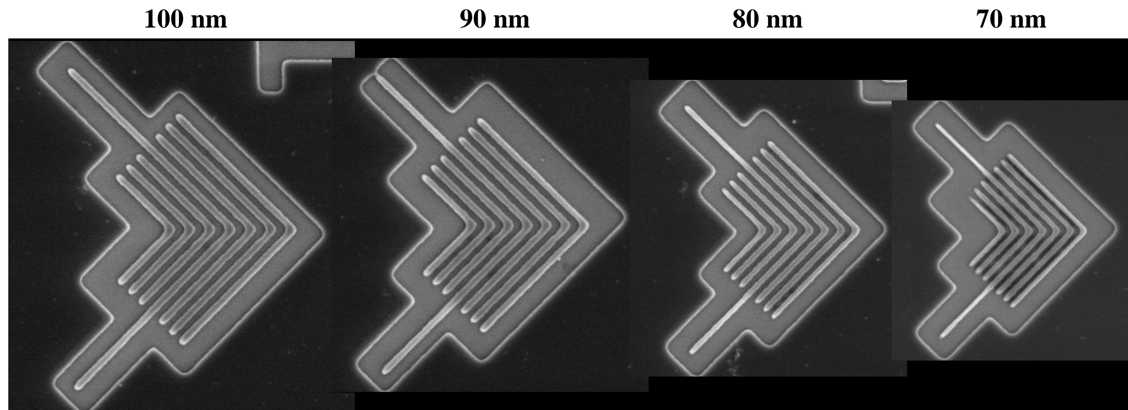

Fig. 9. Series of elbow images ranging from 100 to 70 nm printed with the scanning illuminator set to model in the ETS 6-channel pupil fill.

In Fig. 7 equal line-space printing down to 50-nm is demonstrated, which was achieved using dipole illumination (Fig. 3) to improve the resolution in the vertical direction at the expense of other orientations. In the case of resolution enhancing illumination, this represents a k_1 factor of 0.37 for dense line features. The 0.25-NA equivalent CD would be 20 nm.

In addition to using resolution-enhancing illuminations, it is also possible to decrease k_1 for loose-pitch features through dose control. Figure 8 shows 39-nm 3:1 pitch elbows printed by

overdosing features coded as 80-nm 1:1 on the reticle. These results were obtained using conventional disk illumination with a partial coherence of 0.7.

As described above, the SES scanning illuminator enables the modeling of stepper-specific pupil fills. This capability has been used to investigate the Set-2 optic imaging performance with the actual ETS 6-channel pupil fill (Fig. 3). Figure 9 shows a series of elbow images ranging from 100 to 70 nm printed in the ETS configuration. Even with the sparse ETS pupil fill, excellent printing performance is observed.

5. SUMMARY

The EUV PS/PDI has been successfully upgraded to now include static microfield printing capabilities. To accurately replicate realistic printing conditions, the SES has been equipped with a coherence-controlling illuminator allowing the generation of arbitrary pupil fills. These capabilities have been applied to the print-based characterization of the ETS Set-2 optic. The Set-2 optic, which will subsequently be installed in the ETS, has been demonstrated to have excellent imaging performance, well exceeding its design specification of 100-nm CD. Dense-line resolution down to 50 nm has been demonstrated using dipole illumination and loose-pitch printing down to 39 nm has been demonstrated using conventional illumination. Additionally, good imaging performance has also been demonstrated in conjunction with the ETS 6-channel pupil fill.

6. ACKNOWLEDGEMENTS

The authors are greatly indebted to Kevin Bradley, Rene Delano, Gideon Jones, David Richardson, Ron Tackaberry, and Eugene Veklerov for expert engineering and fabrication support, and to the entire CXRO staff for enabling this research. This research was supported by the Extreme Ultraviolet Limited Liability Company and the DOE Office of Basic Energy Science.

REFERENCES

1. J. H. Underwood and T. W. Barbee, Jr., “Layered synthetic microstructures as Bragg diffractors for X rays and extreme ultraviolet: theory and predicted performance,” Appl. Opt. **20**, 3027-3034 (1981).
2. D. Attwood, G. Sommargren, R. Beguiristain, K. Nguyen, J. Bokor, N. Ceglio, K. Jackson, M. Koike, and J. Underwood, “Undulator radiation for at-wavelength interferometry of optics for extreme-ultraviolet lithography,” Appl. Opt. **32**, 7022-7031 (1993).
3. H. Medecki, E. Tejnil, K. A. Goldberg, and J. Bokor, “Phase-shifting point diffraction interferometer,” Opt. Lett. **21**, 1526-1528 (1996).
4. K. Goldberg, P. Naulleau, J. Bokor, and H. Chapman, “Honing the accuracy of extreme ultraviolet optical system testing: at-wavelength and visible-light measurements of the ETS Set-2 projection optic,” *these proceedings*.
5. K. A. Goldberg, E. Tejnil, S. H. Lee, H. Medecki, D. T. Attwood, K. H. Jackson, and J. Bokor, “Characterization of an EUV Schwarzschild objective using phase-shifting point diffraction interferometry,” Proc. SPIE Vol. **3048**, 264-70 (1997).
6. P. Naulleau, K. Goldberg, S. Lee, C. Chang, D. Attwood, and J. Bokor, “Extreme-ultraviolet phase-shifting point diffraction interferometer: a wave-front metrology tool with sub-angstrom reference-wave accuracy,” Appl. Opt. **38**, 7252-7263 (1999).
7. K. A. Goldberg, P. Naulleau, P. Batson, P. Denham, H. Chapman, and J. Bokor, “Extreme ultraviolet alignment and testing of a four mirror aspheric extreme ultraviolet optical system,” J. Vac. Sci. and Technol. B **18**, 2911-15 (2000).

8. D. A. Tichenor, G. D. Kubiak, M. E. Malinowski, R. H. Stulen, S. J. Haney, K. W. Berger, R. P. Nissen, R. L. Schmitt, G. A. Wilkerson, L. A. Brown, P. A. Spence, P. S. Jin, W. C. Sweat, W. W. Chow, J. E. Bjorkholm, R. R. Freeman, M. D. Himel, A. A. MacDowell, D. M. Tennant, O. R. Wood II, W. K. Waskiewicz, D. L. White, D. L. Windt, and T. E. Jewell, "Development and characterization of a 10× Schwarzschild system for SXPL," in *OSA Proceedings on Soft X-Ray Projection Lithography,* Vol. **18**, A. M. Hawryluk and R. H. Stulen, eds., (Optical Society of America, Washington, DC, 1993), pp. 79-82.
9. D. W. Sweeney, R. Hudyma, H. N. Chapman, and D. Shafer, "EUV optical design for a 100 nm CD imaging system," in *Emerging Lithographic Technologies II*, Y. Vladimirsky, ed., Proc. SPIE **3331**, 2-10 (1998).
10. D. Tichenor, W. Replogle, S. Lee, W. Ballard, G. Kubiak, L. Klebanoff, J. Goldsmith, J. Wronosky, L. Hale, H. Chapman, J. Taylor, K. Goldberg, P. Naulleau "Performance upgrades in the EUV Engineering Test Stand," *these proceedings*.
11. S. Lee, D. Tichenor, W. Replogle, H. Chapman, L. Bernardez, W. Ballard, A. Leung, D. O'Connell, E. Panning, J. Bjorkholm, C. Gwyn, "Lithographic evaluation of the EUV engineering test stand," *these proceedings*.
12. P. Naulleau, K. Goldberg, E. Anderson, P. Batson, P. Denham, S. Rekawa, and J, Bokor, "At wavelength characterization of the Engineering Test Stand Set-2 optic," J. Vac. Sci. & Technol. B **19**, 2396-2400 (2001).
13. D. Attwood, P. Naulleau, K. Goldberg, E. Tejnil, C. Chang, R. Beguiristain, P. Batson, J. Bokor, E. Gullikson, H. Medecki, and J. Underwood, "Tunable coherent radiation in the soft X-ray and extreme ultraviolet spectral regions," IEEE J. Quantum Electron. **35**, 709-720 (1999).
14. C. Chang, P. Naulleau, E. Anderson, and D. Attwood, "Spatial coherence characterization of undulator radiation," Opt. Comm. **182**, 25-34 (2000).
15. P. Naulleau, K. Goldberg, E. Anderson, P. Batson, P. Denham, S. Rekawa, and J. Bokor, "Adding static printing capabilities to the EUV phase-shifting point diffraction interferometer," Proceedings of the SPIE Vol. **4343**, 639-645 (2001).
16. J. W. Goodman, *Statistical Optics*, John Wiley & Sons, New York, 1986.